Available online at www.sciencedirect.com
SCIENCE DIRECT®
Acta Materialia 52 (2004) 2005–2012
Acta MATERIALIA
www.actamat-journals.com

Cold rolling behaviour of an austenitic Fe–30Mn–3Al–3Si TWIP-steel: the importance of deformation twinning

S. Vercammen [a,*], B. Blanpain [a,*], B.C. De Cooman [b], P. Wollants [a]

[a] K.U.Leuven, Department of Metallurgy and Materials Engineering, Kasteelpark Arenberg 44, B-3001 Leuven, Belgium
[b] Laboratory for Iron and Steelmaking, Ghent University, Technologiepark 903, B-9052 Ghent, Belgium

Received 24 September 2003; received in revised form 23 December 2003; accepted 29 December 2003

Abstract

The present paper deals with the evolution of microstructure and texture of a TWIP-steel during cold rolling. With increasing strains, different deformation mechanisms become active. TEM observations show the presence of deformation twinning at low strains ($\varepsilon < 0.1$). As the strain increases the volume fraction of twins increases. At higher strain levels, non-homogeneous deformation mechanisms such as shear band formation become active. This evolution of the microstructure is reflected in the formation of the texture. The brass orientation $\{1\,1\,0\}\langle 1\,1\,2\rangle$ is dominant at every strain level. Its intensity increases as strain increases, while additional texture components develop at different strain levels: the E $\{1\,1\,1\}\langle 1\,1\,0\rangle$ and F orientation $\{1\,1\,1\}\langle 1\,1\,2\rangle$ as well as the S orientation $\{1\,2\,3\}\langle 6\,3\,4\rangle$. Compared to these orientations the copper orientation intensity remains rather low.

Keywords: Twinning; Texture; Cold rolling; TEM; Stacking fault energy

1. Introduction

The development of steels for a variety of automotive applications is focused on an increase of strength combined with the preservation or improvement of its formability. The increase of strength enables car manufacturers to reduce the weight of the car, whereas the increase of ductility allows for more complex car design. Dispersed phase steels such as transformation induced plasticity (TRIP) steels combine these properties, making them very attractive for the automobile industry. Their product of ultimate tensile strength and elongation to failure-ductility-value can be as high as 25,000 MPa%. Homogeneous austenitic steels, alloyed with C, Cr, Ni, Mo, Mn and Si have even higher R_mA-values: 35,000–40,000 MPa% [1]. The high work hardening plays a dominant role during deformation and results in excellent mechanical properties. The mechanisms, responsible for this high work hardening, are related to the stacking fault energy (SFE) of the austenitic phase. The SFE changes with the alloy composition and the deformation temperature. Its magnitude controls the ease of cross-slip, and thus different deformation mechanisms can be activated at different stages of deformation [2,3]. As the SFE decreases the stacking faults become wider and cross-slip more difficult and mechanical twinning is favoured.

Most austenitic steels, such as austenitic stainless steels [4] and high manganese Hadfield steels [5], have low-to-moderate SFE and therefore tend to form extended stacking faults, deformation twins and planar dislocation structures. These different lattice defects strongly influence the stress strain response and the evolution of the texture during cold rolling.

Extensive mechanical twinning is observed in austenitic high manganese steels alloyed with carbon [6] or alloyed with aluminium and silicon [7]. Grässel et al. [7] observed that mechanical twinning becomes dominant when the Mn content reaches 25 wt%, the Al content is higher than 3 wt% and the Si content is between 2 and 3 wt%, and when the C content is low. They reported high R_mA-values of over 50,000 MPa%; these values were

* Corresponding authors. Tel.: +32-163-211-83; fax: +32-163-219-91.
E-mail addresses: steven.vercammen@mtm.kuleuven.ac.be (S. Vercammen), bart.blanpain@mtm.kuleuven.ac.be (B. Blanpain).

1359-6454/$30.00 © 2004 Acta Materialia Inc. Published by Elsevier Ltd. All rights reserved.
doi:10.1016/j.actamat.2003.12.040

largely due to a very high ductility, $A = 80\%$. They introduced the term twinning induced plasticity (TWIP).

The aim of this research is to obtain a better insight in the active deformation mechanisms of FeMnAlSi TWIP-steels during cold rolling in order to assess their potential as strip products. A Fe–30Mn–3Al–3Si TWIP-alloy was cast, hot rolled and annealed. Subsequently, the alloy was cold rolled with different degrees of deformation. The evolution of the microstructure was analysed by means of light optical microscopy and transmission electron microscopy (TEM). The different deformation mechanisms – especially mechanical twinning – were visualised. The effects of these mechanisms was analysed by crystallographic texture measurements. Orientation intensity and volume fraction plots at different cold rolling strains help to monitor the overall orientation evolution of the grains in the material during the process.

2. Experimental procedure

2.1. Material

The alloy was melted in a vacuum induction furnace and ingot cast (290 mm × 250 mm × 120 mm). The chemical composition of the alloy, measured by inductively coupled plasma mass spectrometry (ICP-MS) using the standard addition method, is given in Table 1. A 11.2 mm thick plate was cut from the ingot, homogenised in an air furnace at 1200 °C, hot rolled at 1100 °C in a single pass to a thickness of 7 mm ($\varepsilon = 0.47$) and coil cooled in a furnace from 600 °C (T_0) following an imposed exponential temperature decrease: $T = T_0^{(\frac{100}{100+t})}$, where T is the temperature in °C and t is the time in hours. The factor (1 0 0) in the exponent exhibits the unit hours.

2.2. Cold rolling procedure

Eight samples were cut from the hot rolled and annealed plate and cold rolled at room temperature using a laboratory rolling mill equipped with a roll diameter of 200 mm. The rolling direction was the same as for the hot rolling. The cold rolling was done without reversing the rolling direction and a lubricant was applied on the rolls. Details of the rolling procedure are given in Table 2.

Table 1
Chemical analysis of the TWIP-steel (wt%) determined by ICP-MS

C	Mn	Si	S	Al	Fe
0.0049	29.4	3.0	0.0033	3.3	Balance

2.3. Microscopy

Samples were taken from the hot rolled and annealed plate. They were polished and etched at room temperature using a two stage etching procedure [8] to reveal the grain boundaries. Specimens for TEM were cut out at the centre of three cold rolled samples along the longitudinal direction ($\varepsilon = 0.10$, 0.21 and 1.05). They were mechanically polished to a thickness of 0.1 mm. Thin foils were prepared using a double jet TENUPOL-3 electrolytic polisher at a voltage of 32 V and a temperature between 10 and 15 °C. The electrolyte contained 5 vol% of perchloric acid and 95 vol% of acetic acid. The thin foils were examined in a CM-200 FEG Philips TEM equipped with a Schottky field emitter. The TEM was operated at an acceleration voltage of 200 kV.

2.4. Texture determination

Quantitative texture measurements were performed by X-ray diffraction with $Cu_{K_{\alpha_1}}$ radiation. On the centre layer of all cold rolled specimens four incomplete ($0° < \alpha < 80°$) pole figures ({1 1 1}, {2 0 0}, {2 2 0} and {1 1 3}) were measured in the back reflection mode by using a fully automated Siemens D500 texture goniometer and using $Cu_{K_{\alpha_1}}$ radiation. The orientation distribution functions (ODFs) were calculated from the four measured and corrected pole figures using the series expansion method [9–11]. In addition the volume fractions of the most important orientation components were calculated directly from the experimentally measured pole figures using a spread of 16.5° around the exact position.

3. Results

3.1. Microstructure

The hot rolling and annealing treatment resulted in a fully austenitic microstructure as can be deduced from

Table 2
Parameters of the cold rolling process

Sample	1	2	3	4	5	6	7	8
True strain $\varepsilon = \ln\left(\frac{t_0}{t}\right)$	0.1	0.21	0.43	0.69	1.05	1.39	1.90	2.30
Engineering strain $\rho = \frac{t_0 - t}{t_0}$	0.10	0.20	0.35	0.50	0.65	0.75	0.85	0.90
Number of passes	6	11	21	31	44	53	65	100

diffraction analyses. The microstructures of the as hot rolled and annealed samples show more or less equiaxial austenitic grains with a significant amount of coherent annealing twins (Fig. 1). The average grain size is about 40 μm.

Based on the chemical composition (Table 1) of the TWIP-steel the SFE has been estimated by thermodynamic calculations [7] and also using an empirical formula based on X-ray diffraction line profiles and regression analysis of commercial austenitic stainless steels [12]. Both methods result in nearly the same value of about 40 mJ/m^2. Mechanical properties of the hot rolled annealed TWIP material are given in Table 3. A high product of ultimate tensile strength and elongation to failure-value of about 40,000 MPa has been obtained.

Besides the profuse presence of annealing twins (Fig. 1) the hot rolled and annealed samples contain many stacking faults (SF), consistent with the calculated value of the SFE (Fig. 2). The type of the SFs in the material was determined from the nature of outer thickness fringes following the two-beam bright field (BF)/axial dark field (ADF) imaging procedure of Fultz and Howe [13]. The SFs were characterised as extrinsic type of SFs (Fig. 3).

At a cold rolling strain of $\varepsilon = 0.10$ straight deformation twins are already present in more than 50% of the grains (Fig. 4). Generally, only one twinning system is active in each grain; the twinning system having a suitable orientation with respect to the rolling direction; twins formed on {1 1 1} planes with maximum resolved shear stress. Grains without mechanical deformation twins contain a high density of planar dislocation structures (Fig. 4). At a degree of deformation 0.21, nearly every grain has accommodated the strain by activating a twinning system (Fig. 5). Twinning as primary deformation mechanism leads to nanoscale layered structures because of the small thickness of the twins (between 100 and 50 nm see Fig. 5 top left). In between the mechanical twins dislocations are formed. In some cases a second set of twins is observed. At $\varepsilon = 0.10$ the twins appear as straight lines. At $\varepsilon = 0.21$ the previously formed twin boundaries tend to bend towards the rolling direction. At large strains it is difficult to observe the active deformation mechanisms in the grains because of the elongation and the fragmentation of the grains. TEM observations show a band like lamellar structure for a rolling strain of 1.05 (Fig. 6). Some of these lamellae contain twins. Neither XRD measurements nor TEM observation revealed the presence of ε- or α-martensite before and after cold rolling.

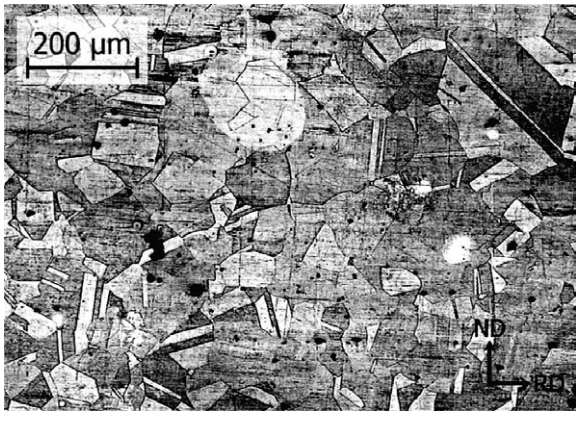

Fig. 1. Longitudinal section of the as hot rolled and annealed TWIP-steel revealing equiaxied grains containing annealing twins (etched).

Table 3
Mechanical properties of the TWIP-steel measured in a uniaxial tensile test

YS (MPa)	UTS (MPa)	E (GPa)	A (%)	n (–)
300	650	189	60	0.41

3.2. Texture evolution

From the $\varphi_2 = 45°$ sections of the orientation distribution functions (Fig. 7) calculated for the eight cold

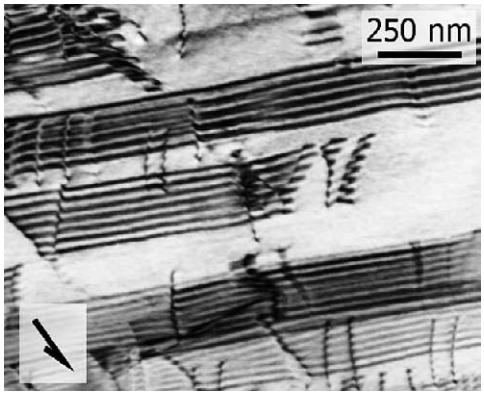

Fig. 2. Two-beam BF image of overlapping SFs in the as hot rolled annealed alloy (zone axis [0 1 1] and $g = (0\,2\,\bar{2})$).

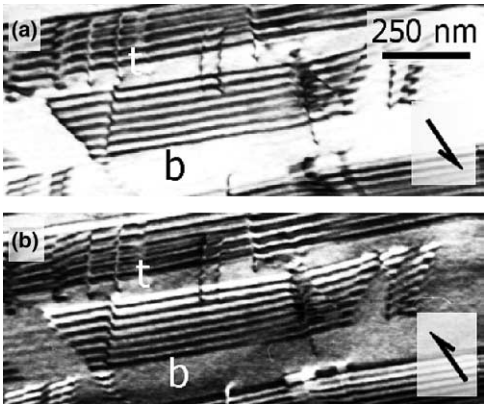

Fig. 3. Two-beam BF and ADF image of a SF, indicating top and bottom of the specimen and the extrinsic nature of the fault (zone axis [0 1 1] and $g = (0\,2\,\bar{2})$ (a) and $g = (0\,\bar{2}\,2)$(b)).

rolling strains (Fig. 2), the rolling texture can generally be interpreted as being essentially a brass-type texture $\{1\,1\,0\}\langle 1\,1\,2\rangle$ with a spread towards the Goss-type texture $\{1\,1\,0\}\langle 0\,0\,1\rangle$. Besides these orientations other important texture components (Table 4, Figs. 8 and 9) are situated in these sections, except for the S-orientation lying on the β-fibre, which is the so-called skeleton line of the texture and of great importance for fcc materials (Fig. 9).

As the rolling strain increases the intensity of the brass orientation increases gradually resulting at $\varepsilon = 2.30$ in a total volume fraction of about 35% (using a spread

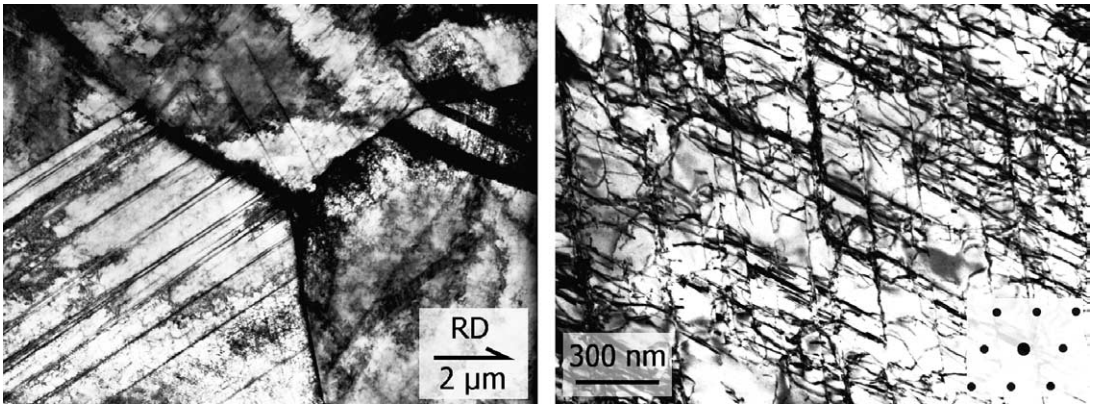

Fig. 4. $\varepsilon = 0.10$: BF images of the as cold rolled material. The left picture shows several grains, some of them containing mechanical twins (as can be seen in the bottom left grain). Grains that do not twin contain dislocations (right picture).

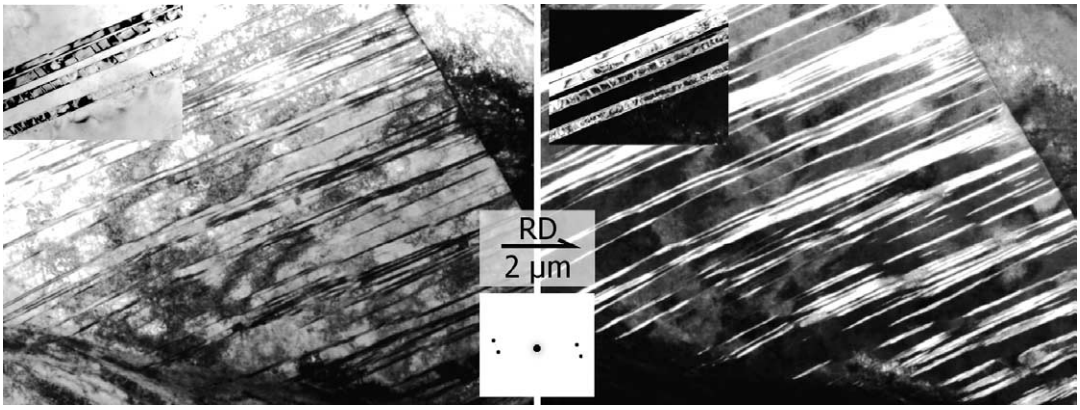

Fig. 5. $\varepsilon = 0.21$: BF (left) and ADF (right) $g = (1\,1\,1)$ images of the as cold rolled material. The diffraction pattern (extra points) gives evidence of the presence of twins. A detail (×50) of the twins inside the grain is represented in the insets at the top left (volume fraction of the twins in this grain: ~20%).

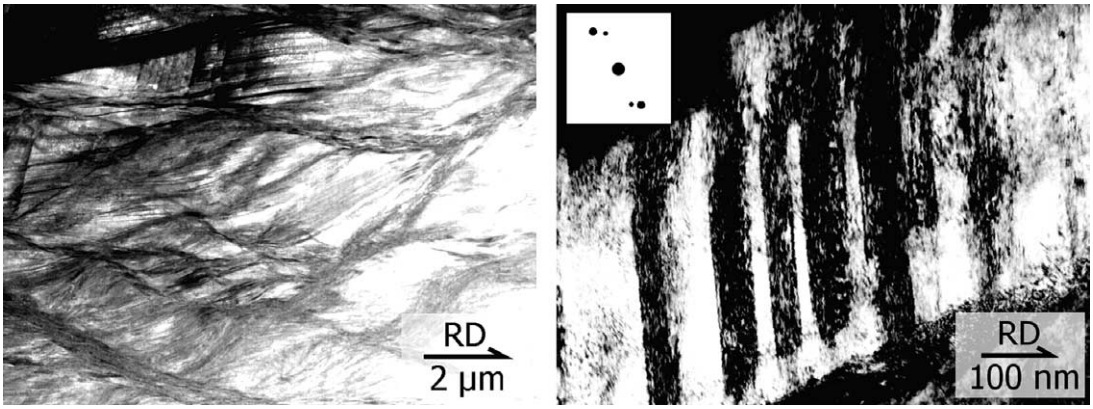

Fig. 6. $\varepsilon = 1.05$: BF images of the as cold rolled material revealing S-shaped lines: shear bands (left), some of them containing twins (right: see diffraction pattern).

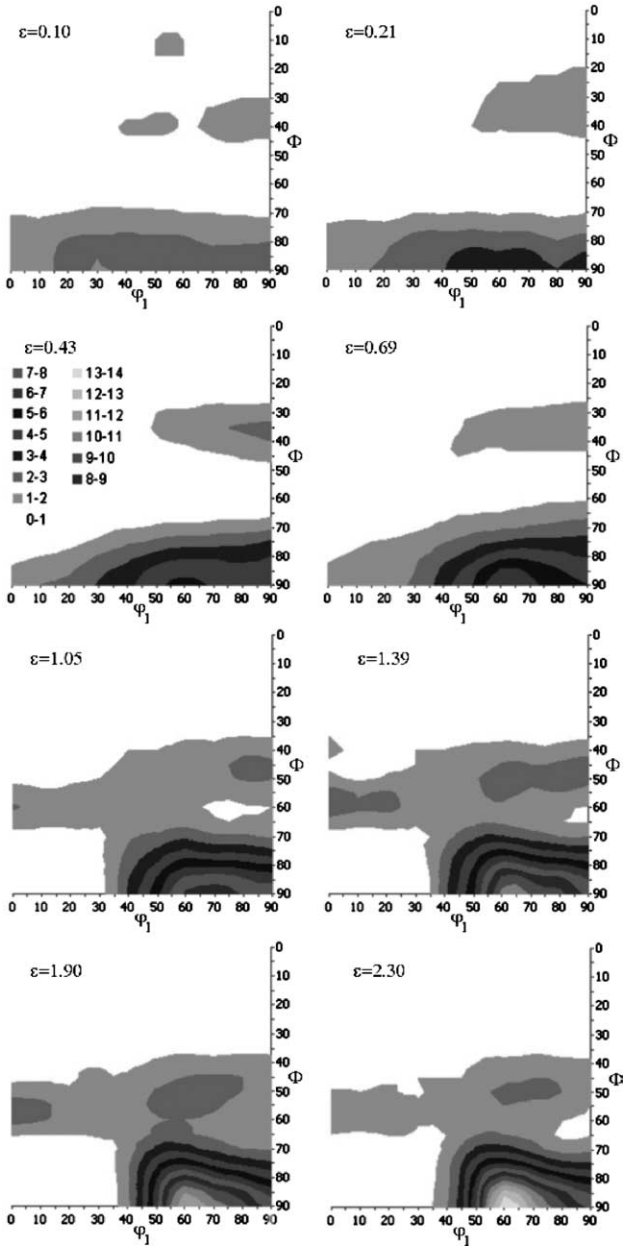

Fig. 7. Evolution of texture during cold rolling: $\varphi_2 = 45°$ sections of the ODFs of the TWIP-alloy for various rolling strains.

of 16.5° around the ideal orientation: Fig. 9(b)) being the most intense crystal orientation in the material. The volume fraction of crystals with the S orientation $\{1\,2\,3\}\langle 6\,3\,4\rangle$ increases also with a similar rate in the early stages of cold rolling but seems to saturate at strain levels of 1.0. Besides, the position of the skeleton line (β-fibre) evolves during deformation towards higher ϕ values. The increase of intensity followed by saturation is also true for the Goss (on the α- and τ-fibre) and the copper twins orientations $\{5\,5\,2\}\langle 1\,1\,5\rangle$ (on the τ-fibre). However, their volume fraction is clearly smaller. From the evolution of the α-fibre it is clear that only few crystals tend to orient themselves in a copper orientation

Table 4
Important crystallographic orientations of textured pure fcc metals and alloys, their orientation, presence in a fibre and Euler angles at $\varphi_2 = 45°$

Name	Orientation	Fibre	Euler angles: $g = [\varphi_1\,\phi\,45]$
C, cube	$\{0\,0\,1\}\langle 1\,0\,0\rangle$	–	[45 0 45]
G, Goss	$\{1\,1\,0\}\langle 0\,0\,1\rangle$	ατ	[90 90 45]
B, brass	$\{1\,1\,0\}\langle 1\,1\,2\rangle$	αβ	[55 90 45]
RG, rot. Goss	$\{1\,1\,0\}\langle 1\,1\,0\rangle$	α	[0 90 45]
E	$\{1\,1\,1\}\langle 1\,1\,0\rangle$	γ	[0 55 45] [60 55 45]
F	$\{1\,1\,1\}\langle 1\,1\,2\rangle$	γ	[30 55 45] [90 55 45]
Cu, copper	$\{1\,1\,2\}\langle 1\,1\,1\rangle$	βτ	[90 35 45]
CuT, copper twins	$\{5\,5\,2\}\langle 1\,1\,5\rangle$	τ	[90 74 45]
S	$\{1\,2\,3\}\langle 6\,3\,4\rangle$	β	[59 37 63]

α-fibre: ⟨1 1 0⟩ parallel to ND
β-fibre: ⟨1 1 0⟩ tilted 60° from ND towards RD
γ-fibre: ⟨1 1 1⟩ parallel to ND
τ-fibre: ⟨1 1 0⟩ parallel to TD.

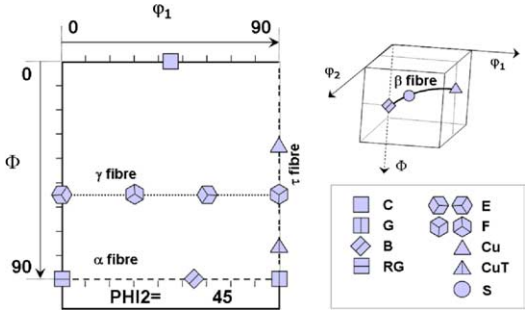

Fig. 8. Schematic representation of the important orientations in fcc materials.

$\{1\,1\,2\}\langle 1\,1\,1\rangle$. On the exact copper position the intensity increases a little bit, reaching a maximum at $\varepsilon = 0.43$ (see also the volume fraction evolution in Fig. 9(b)) and decreasing at higher strain levels: $\varepsilon > 0.50$. A closer look at the α-fibre shows actually a shift on the copper peak to $\phi = 55°$. This tendency matches with the construction of a γ-fibre where both the E $\{1\,1\,1\}\langle 1\,1\,0\rangle$ and the F orientation $\{1\,1\,1\}\langle 1\,1\,2\rangle$ are situated. Their volume fraction increases remarkably in between $\varepsilon = 0.43$ and $\varepsilon = 0.69$ and seems to saturate at high strain levels.

4. Discussion

Generally, TEM observations and texture evolution correspond to the behaviour of other low-to-moderate SFE fcc materials such as stainless steels, Hadfield steels or Cu–Zn alloys with Zn content >25%. The presence of annealing (or growth) twins (Fig. 1) in the hot rolled and annealed material gives already evidence of the low value of the SFE (40 mJ/m^2) [4,14]. In addition, a large number of wide SFs have been observed in TEM (Fig. 2), as may be expected for a low SFE material. Extrinsic SFs are not so common [15]. They may result

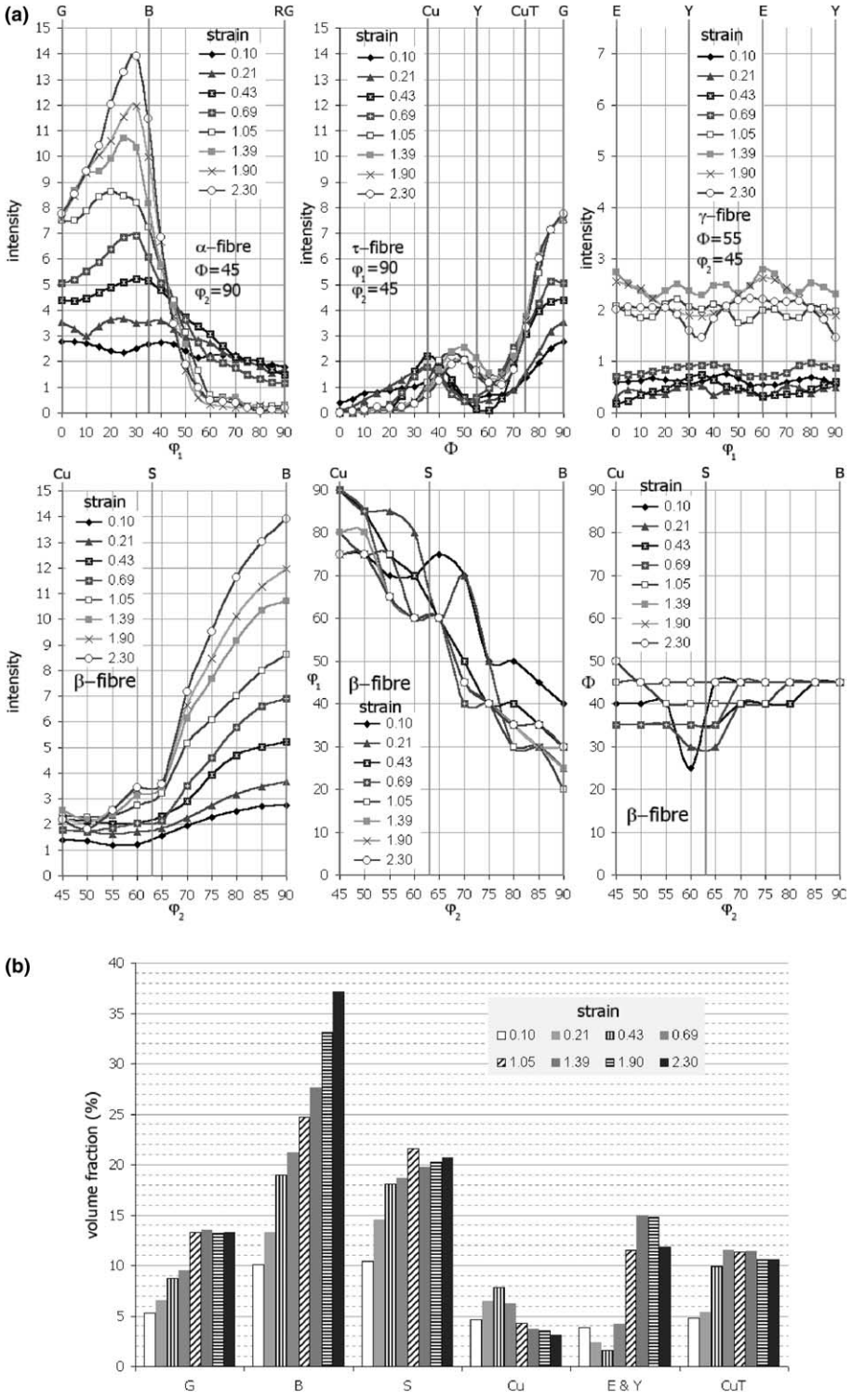

Fig. 9. Evolution of the (a) different fibres and (b) volume fraction of important orientations using a spread of 16.5° around the exact position.

from different mobilities for the leading and trailing partial dislocations due to a difference in the resolved shear stresses of the partials or due to pinning of partials by forest dislocations or kinks. The alloying elements in solid solution might also act as favourable elements in reducing the dislocation mobility or raising the shear stress for slip [6]. It should be noted that the presence of extrinsic ESFs (Fig. 3), has also been reported in recent studies on Hadfield steels [16]. This is consistent with the occurrence of deformation twins during straining (see below) because ESFs can be seen as preferential twin nuclei.

Similarly as for Hadfield steels [5], twinning is observed as the primary deformation mechanism of the TWIP-steel at the onset and early stage of cold rolling. The SFs act as preferential nuclei and not much glide is necessary before mechanical twins start to form. At a degree of deformation of 0.10, 50% of the grains contain twins. This behaviour differs from other low SFE fcc metals because the twinning in these materials is preceded by the activation of multiple slip systems [17]. At cold rolling strains of about 20% twins start to form in brass Cu–30Zn [18]. Chowdhury et al. [14] report profuse twinning after 40% cold reduction in a AISI 316 stainless steel with an initial grain size within the range of 70–100 μm, whereas Aernoudt et al. [19] report twinning in drawn silver wires with initial grain size of 200 μm after 48% reduction of cross-section.

The primary occurrence of deformation twins in the TWIP-steel at $\varepsilon = 0.10$ is reflected in the growth retardation, i.e. the weak intensity, of the copper orientation (Fig. 9) and the formation of a moderate α-fibre. This reduction in the density of the copper orientation, which initiates the formation of the brass-type texture, is known to be caused by mechanical twinning, by which the copper orientation is transformed to a position near the Goss orientation, the copper twin orientation rotating into the Goss orientation. Consequently, the Goss and copper twin orientations increase their intensity gradually (τ-fibre in Fig. 9) while increasing the strain, as the amount of mechanical twins increases drastically. In addition, the twins start to bend towards the rolling direction. This is due to the local accommodation of strain in the grains, similarly to crystal lattice bending.

At the saturation of the Goss and the copper twin orientations the γ-fibre develops as can be seen in Fig. 9. The increase of the E and the F orientations stems from the rotation of {1 1 1} into the rolling plane. This is believed to be a result of preferential slip on {1 1 1} planes common to the twin plane, coplanar slip [18], because of the small thickness of the twin lamellae shortening the dislocation path for other slip systems. Likewise, such behaviour results in an increase of ϕ on the β-fibre (a shift of the copper orientation towards higher ϕ values, Fig. 9).

At very high strain levels the deformation becomes inhomogeneous as shear bands become visible (Fig. 6). These bands are oriented at +35° and −35° to the RD and are often referred to as a fish bone structure. This behaviour is a result of the inhibition of crystallographic slip as: (i) most of the grains are twinned and their twinning planes have been reoriented parallel to the rolling plane resulting in very low Schmid factors on these slip systems and (ii) slip on other systems is limited. These grains make continued homogeneous deformation difficult and shear banding becomes the dominant deformation mechanism [20].

Finally, it was also found that the mechanical properties (Table 3) were comparable to those mentioned by Grässel at al. [7]. The twinning deformation mode plays a very important role as it results in an extra strain hardening due to the static hardening effect of twin boundaries acting as strong barriers to slip propagation.

5. Conclusion

Both TEM observation (direct) and texture analysis (indirect) show the evolution of the different deformation mechanisms, which are active at different cold rolling strains. The investigated high manganese TWIP-steel exhibits a pronounced brass-type texture evolution already at low strain levels. The latter is a very stable texture component in rolling deformation when octahedral slip and mechanical twinning are active deformation mechanisms. No pronounced copper orientation develops. This behaviour stems from the early formation of deformation twins in the material, similarly detected in Fe–Mn–C Hadfield steels, and is related to the low SFE of the material (40 mJ/m^2). Indeed, TEM pictures reveal the presence of a non-negligible amount of deformation twins at low strains. The twinned fraction increases with increasing strain and consequently the Goss and copper twin orientation develop. At higher strains E and F are present. This is very likely due to the alignment of twin lamellae parallel to the rolling plane. It is believed that twinning acts as the primary deformation mechanism in this low SFE austenitic TWIP-steel, leading to nanoscale layered structures, resulting in extreme mechanical properties.

Acknowledgements

Discussions with professors E. Aernoudt, B. Verlinden and with M. Seefeldt were most helpful and very much appreciated. This work was: (i) supported by the Institute for the Promotion of Innovation through Science and Technology in Flanders (IWT) under Grant SB/1163 and (ii) carried out under the Interuniversity attraction poles programme financed by the Belgian State, Federal office for scientific, technical and cultural affairs, contract P8/05.

References

[1] Pickering FB. Physical metallurgical development of stainless steels, In: Proceedings Conference Stainless Steels 84, Gothenburg, 1984, p. 2–281.
[2] Christian JW, Mahajan S. Deformation twinning. Prog Mater Sci 1995;39:1–157.
[3] Olson GB, Owen WS. Martensite. Ohio: ASM International; 1992.

[4] Donadille C, Valle R, Dervin P, Penelle R. Development of texture and microstructure during cold-rolling and annealing of FCC alloys: example of an austenitic stainless steel. Acta Metall 1989;37(6):1547–71.
[5] Adler PH, Olson GB, Owen WS. Strain hardening of hadfield manganese steels. Metall Trans A 1986;17A:1725–37.
[6] Tsakiris V, Edmonds DV. Martensite and deformation twinning in austenitic steels. Mater Sci Eng A 1999;A273–275:430–6.
[7] Grässel O, Frommeyer G, Derder C, Hofmann H. Phase transformation and mechanical properties of Fe–Mn–Si–Al TRIP-steels. J Phys IV France 7 1997;C5:383–8.
[8] Schumann H, Goodknecht K. Metallographischer nachweis von hexagonalem epsilon-martensit in austenitischen manganstählen. Prakt Met 1966;3:147–53.
[9] Van Houtte P. A new method for the determination of texture functions from incomplete pole figures – comparison with older methods. Texture Microstruct 1984;6:137–62.
[10] Van Houtte P. A method for the generation of various ghost correction algorithms – the example of the positivity method and the exponential method. Texture Microstruct 1991;13:199–2128.
[11] Bunge HJ. Texture analysis in materials science. London: Butterworth; 1982.
[12] Schramm RE, Reed RP. Stacking fault energies of seven commercial austenitic stainless steels. Metall Trans A 1975;6A:1345–51.
[13] Fultz B, Howe J. Transmission electron microscopy and diffractometry of materials. Berlin: Springer; 2001.
[14] Chowdhury SG, Das S, Ravikumar B, Kumar S, Gottstein G. Textural development in IASI 316 stainless steel during cold rolling and annealing. Mater Sci Forum 2002;408–412:1371–6.
[15] Mahajan S. The evolution of intrinsic–extrinsic faulting in fcc crystals. Metall Trans A 1975;6A:1877–86.
[16] Karaman I, Sehitoglu H, Chumlyakov YI, Maier HJ, Kireeva IV. Extrinsic stacking faults and twinning in hadfield manganese steel single crystals. Scripta Mater 2001;44:337–43.
[17] Nabarro FRN. In: Dislocations in solids, vol. 9. Amsterdam: Elsevier Science; 1992.
[18] Hirsch J, Lücke K, Hatherly M. Mechanism of deformation and development of rolling textures in polycrystalline fcc metals: III the influence of slip inhomogeneities and twinning. Acta Metall 1988;36:2905–27.
[19] Aernoudt E, Kokubo I, Stüwe H-P. Zyklische texturen gezogener silberdrähte. Z Metallkund 1966;57:216–20.
[20] Leffers T. The brass-type texture once again. Proc ICOTOM 1996;11:299–306.